

# CHASSIS DESIGN OF A MOBILE ROBOT FOR REDUCING WEIGHT BY EXCLUDING SUSPENSION ELEMENTS

Submitted: 31<sup>st</sup> December 2014; accepted: 22<sup>nd</sup> February 2015

Tokuji Okada, Nobuharu Mimura, Toshimi Shimizu

DOI: 10.14313/JAMRIS\_2-2015/17

## Abstract:

*This paper proposes the design concept that prevents its total weight from increasing. The object of the methodology is to modify a conventional robot chassis for structural simplicity by composing the chassis from an elastic material so that it can reduce vibration and shock to the body. This idea makes it unnecessary to attach additional elements, such as suspension units; in addition, it means that it is possible to easily deform the chassis by forming long holes, and to decrease the total weight of the robot, even when the chassis is thick enough for functionality. It contributes to preventing the weight of the power source from increasing. Structural models for analyzing flexure of the chassis using the finite element method (FEM) are pursued. Also, dynamic behaviors of the chassis are clarified based on the modal analysis. The minor difference in error between the experimental and analytical data verifies that the models are useful in a practical application.*

**Keywords:** mobile robot, chassis flexure, suspension-less, FEM, wheelchair

## 1. Introduction

Suspension is a general term of the equipments transforming forces and moments from the wheel to the vehicle body. Its principal functions can be briefly stated as that they must isolate its main body from the vibration caused by various road conditions. The equipments are necessary to the comfort of passengers on vehicles moving with high speed [1].

Normally, the mobile robots need to be rigid for strengthening purposes in their structures to support the total weight of power sources, actuators, controllers, etc., in addition to the weight of a driver and cargo, in need. In addition, the robot is obliged to decrease vibration and shock to move smoothly on an irregular surface by the attachment of mechanical elements, such as suspensions and shock absorbers, at the bottom of its body [2]. Therefore, the robot body, say *chassis*, becomes heavy due to the installation of these elements.

Small size mobile robots may not need suspension systems since the vibration does not matter as far as its position is satisfactory in controlling. Also, in multi-jointed wheeled or legged robots, the suspension system is not necessary because the robot can change the height of wheels or legs by an up-down motion using the information from a camera system. However, vehicles that are used to carry some loads in an unstructured environment need to reduce vibration

promptly by self absorption at wheels. In particular, skid-steering mobile robots need a suspension system or flexible body so that they can get big traction force always with the wheels or legs [3].

This paper considers a solution to prevent the total weight of a robot from increasing and proposes a method to solve this problem by constructing the robot chassis with a flexible body so that it reduces vibration and shock. This idea makes it unnecessary to attach additional elements, such as suspension units. In addition, the chassis is deformed easily by forming long holes and the robot becomes light in its total weight even if the chassis is thick enough to function. Also, it contributes to preventing the weight of the power source from increasing. A rigid area, say a *rigid frame*, of the chassis is utilized as a platform to be fixed by some apparatus when it is not allowed to deform for measuring, controlling, and driving. Fixing cargo to the body becomes difficult due to deformation of the chassis. However, this is solved by implementing spherical joints that allow free angular and linear shifts.

In the latter half, we verify the effectiveness of the methodology of designing a chassis for an application to wheelchairs [4] that move slowly compared to vehicles, in general. To analyze not only the kinematic structure and deformation of the chassis but also its dynamic behaviors, we use a finite element method (FEM), ANSYS Workbench V14.0, which is commercially available. This package can handle a maximum of 256000 points for meshing an object [5]. Hereinafter, we refer to kinetic and geometrical distortions of a chassis as *stress*  $\sigma$  and *flexure*  $E$ , respectively. Dynamic behaviors of the chassis are clarified based on the modal analysis.

## 2. Traditional Design of a Robot Chassis

To make a robot stand stably, it is important to distribute the total load to its wheels so that no individual wheel bears a disproportionately heavy load. Suspension units attached to each wheel generally have the role of equalizing the load across all wheels, even on irregular surface [2]. Some robots make it possible to share the load between the right and left wheels in a simplified structure of a suspension unit. Traditional designs of a suspension unit are illustrated in Fig. 1 [1]. A coiled-spring is utilized for each in Fig. 1(a). In Figs. 1(b) and (c), multi-layered flat springs are placed length- and widthwise, respectively. In Fig. 1(d), a coiled-spring is coupled with hydraulic cylinders to form leveling or height control units by adjusting the

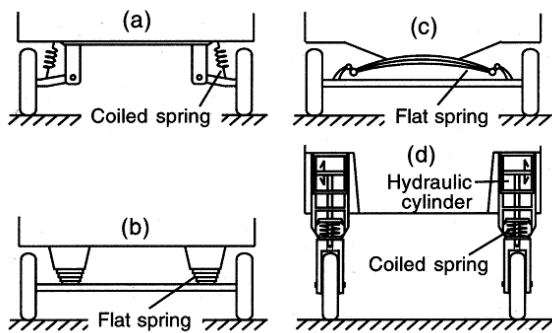


Fig. 1. Traditional designs of a robot chassis

chassis height continuously or step-by-step.

From a kinematics points of view, a suspension system can be expressed as a combination of links and joints. Hence, multi-link suspensions are speculated in Ref. [6], [7], with dynamics analysis of an independent suspension. However, the suspension units attached to the robot chassis make it difficult to decrease the total weight of the robot. In particular, for a robot with leveling or height control units installed, hydraulic or pneumatic power sources must be carried during motion. Consequently, the weight of the robot increases overall.

### 3. Exclusion of Suspension Elements

A chassis is generally equipped with suspension elements to make the robot stand stably on an irregular surface [8]. Noting that we suppose an application to wheelchairs, the chassis is illustrated in Fig. 2(a), where the black outline and spiral mark represent a rigid frame and suspension elements, respectively. The vacant space on the upper side is allotted to a driver for application to a wheelchair. The chassis is elastic in design and parts are removed for flexibility so that it can perform the role of suspension elements. For instance, the chassis has long air space, as shown in Figs. 2(b) and (c). This space is beneficial not only for chassis-flexibility but also for weight-reduction.

#### 3.1. Fundamental Form of a Chassis with Long Air Space

At first, we consider three typical chassis forms. Figs. 2(d)–(f) show them with long air space. We call the form in Fig. 2(d), *BR-type*, since the right and left parts are connected with a narrow band, like a bridge, and the lengthways and sideways loop forms in Figs. 2(e) and (f), *LL-type* and *SL-type*, respectively. Two loop forms are intended to know differences in their kinetic responses. These are all 700 and 500 mm in longitudinal and lateral sizes, respectively. In addition, each removed area is the same in total amount. Other detailed dimensions are not included for brevity.

#### 3.2. Hardening of an Elastic Chassis at its Right and Left Edges

Fig. 3 shows how we make the right and left edges of the chassis rigid; that is, by putting the edges into two angular aluminum channels tightly using screws

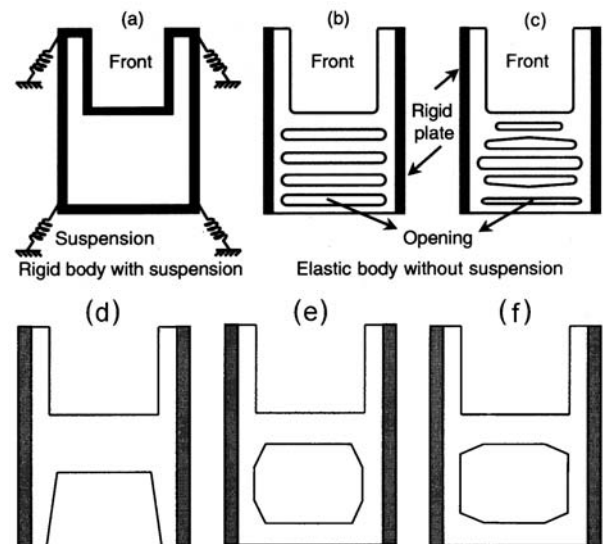


Fig. 2. Rigid chassis using a suspension unit, (a), and suspension-less elastic chassis, (b) and (c). Three simple chassis types, (d), (e), and (f), with some parts of the chassis removed

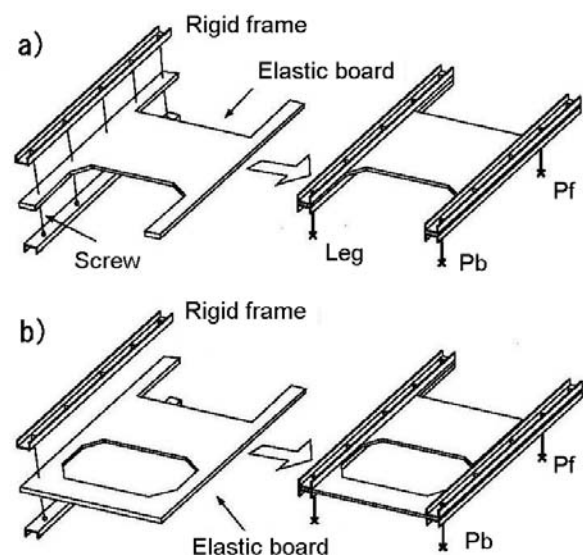
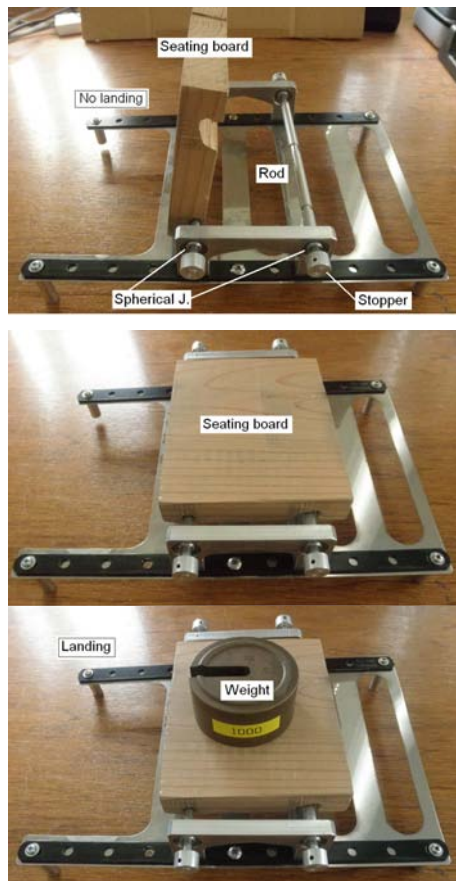


Fig. 3. Fixing of the chassis edges using angular plates for hardening its right and left edges

through several holes. Figs.3(a) and (b) show the assembly of the BR-type and LL-type chassis, respectively.

Driving units are ready to be placed on the rigid frame on the same side as the wheels. Hence, the transmission of driving force is undisturbed by chassis bending, stretching, or twisting. The rigid edges are connected flexibly to create a seating space on the upper side. Fig. 4 shows experimental miniature sets fabricated to verify structural behavior. A pair of rods is guided into spherical joints enabling free axial sliding. The seating board do not distort and the chassis deforms so that the four landing sections remain in con-



**Fig. 4. Flexible landing at four sections by connecting both ends of the chassis using two shafts guided into spherical joints. Chassis frame and seating boards without and with load from the top to bottom, respectively. Front right leg touches the ground only in the bottom figure**

tact the ground with the influence of cargo, even when the ground is rough and uneven terrain.

#### 4. Analysis of a Chassis Flexure Using FEM

The characteristics of flexure versus load at landing sections are necessary to evaluate the function of the chassis suspension. Local and total chassis analyses are important. In addition, total chassis analysis is important because flexure is produced by considering all of the kinetic conditions, such as force, torque, and friction [9]. Ref. [10] helps to understand how the chassis distorts, since it discusses the body movement of a quadruped walking robot. On irregular surface, the center of mass of the robot shifts during motion. This shift may change each of the support forces at the landing sections. To analyze chassis behavior in various conditions on irregular surface, we use a commercially available software [5]. Details on the fundamental and professional applications of the package are provided in Ref. [11].

In general, the load of the driving units operates on the rigid frame directly and the load carried on the upper side operates indirectly via the rods guided into spherical joints. This makes it difficult to deter-

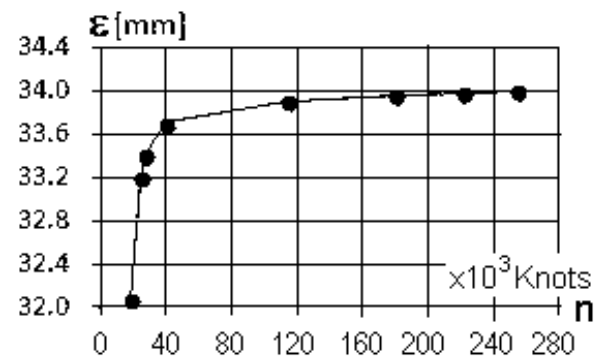


**Fig. 5. Convergence of chassis flexure depending on an increase of finite element knots**

mine the distribution of the sum of these loads and the flexure. Therefore, we suppose that the following three data are given: 1) sum of the load, 2) positions of the four landing sections, and 3) distributed load at each of the landing sections. These make it possible to build a structural model of the chassis, and applying the model to a FEM determines both flexure and stress at an arbitrary point on the chassis.

##### 4.1. Detailed Segmentation of Triangular Surfaces for Using the FEM

To use the FEM, segmentation of an object is important because meshing influences the calculation accuracy and time of results. If the size is particularly small, the accuracy increases, but a long time is required to get the solution, in general. Clearly, the chassis is spacious and the maximum number of knots required to form triangular surfaces is limited on a PC. Therefore, we made clear the relationships between the size, say  $e$ , in mm and the knots, say  $n$ , by using the BR-type chassis of thickness 2 mm (see Fig. 2(d)). The results are such that  $(e, n) = (10, 24360)$ ,  $(6, 39684)$ ,  $(3, 113080)$ ,  $(2.5, 179846)$ ,  $(2.27, 220583)$ ,  $(2.14, 254056)$ . Then, the relationship between  $n$  and  $E$  is correlated, as seen in Fig. 5. These results imply that  $E$  starts to converge at  $n \approx 110000$ ; in other words: at 3 mm in size, and larger values are insignificant to change  $E$ . Therefore, we use 3 mm, except for the special case.

##### 4.2. Chassis Model for Analyzing flexure of a Local Section

We propose the mechanical chassis model shown in Fig. 6. The positive directions of axes (X, Y, and Z) represent rightward, forward, and upward directions, respectively. This model is composed of 4 DOFs (degrees-of-freedom) to make it free of strain, bend, and twist; that is, the center axis passing through the short pivot joint at A allows a motion toward the X-axis direction (sideways) and the rotation around X-axis. In addition, the center axis passing two points B and B' allows a motion toward Y-axis direction (back and forth) and the rotation around Y-axis as a function of the long pivot joint. Four structural legs extending down from the chassis are necessary to analyze flex-

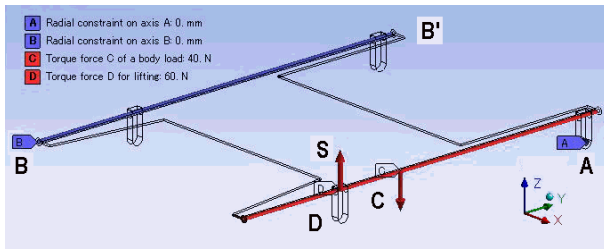


**Fig. 6. Analytical model of a chassis for lifting its right rear section with different force**

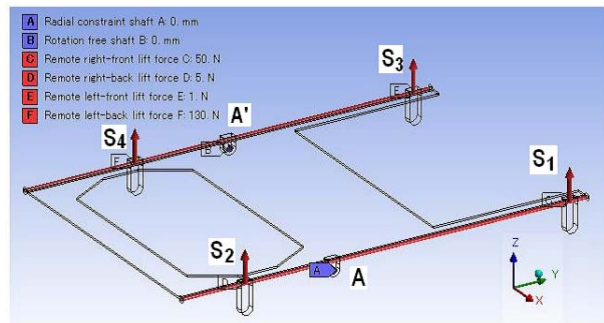


**Fig. 7. Kinematic model of the chassis when it lands on the ground at four sections with a designated load**

ure while a robot standing. Length of each leg is equal to the height of landing sections on the experimental board. It is 40 mm in our experimental set.

Since the total load of the robot presses the chassis against the experimental board, the chassis can move freely if rotation around the joint axis and twist are necessary for seeking a balanced stable condition. Center axis B–B' of the long pivot joint makes the chassis slide and rotate freely in a similar manner to the axis of the short pivot joint. However, the two axes cross at 90°. The downward force at point C is the sum of the load operating on the right side of the rigid frame, and the upward force, S, at point D on the right rear section is the lift force assigned arbitrarily in the calculation. The value of S is bigger than the force to make the leg at its section floated on the ground. The model in Fig. 6 is applicable not only to the BR-type, but also to both the LL-type and SL-type. When we focus on the spring constant at the front, the model is revised by moving the joints to the back and lifting the front so that the two sections are exchanged.

**4.3. Chassis Model for Analyzing interactive flexures at four sections**

Note that the chassis in Fig. 2(e) is selected, the conditions in Fig. 7 are used for the analysis by the FEM, where the positive directions of the X, Y, and Z-axes are the same as those in Fig. 6. Upward arrows at the four landing sections show the support forces operating as torques on each rigid frame. In the condition such that the chassis has no external force between the two rigid parts and four leg ends are free to move on the ground, there is no occurrence of a rotation of the axis CD around the axis EF, and vice versa.

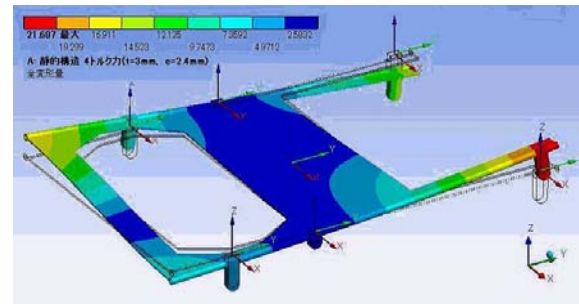
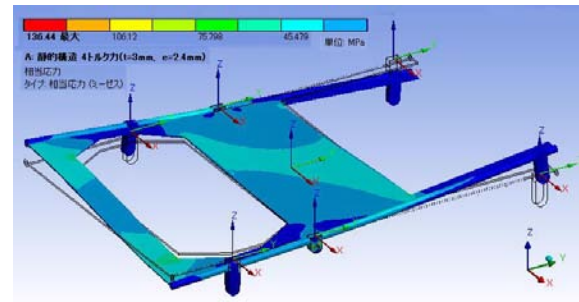


**Fig. 8. Force of stress and chassis flexure calculated under the conditions in Fig. 7 are displayed in the top and bottom, respectively. Results of distortion are contour-banded for ease of visibility**

In short, the axial directions of the pivot joints at each frame are normally parallel, and are aligned when the two concentrated loads operate on symmetrical sections between the right and left.

Therefore, the model in this case allows left and right rigid frames a free pitch motion at the base, where the divided load on both sides operates on each frame concentrically; that is, the two rigid frames have only short pivot joints at A and A' located at almost their middle, without having a B–B' axis. Then, the model behaves completely differently from the previous model. However, there is no difference in the freedom of generating flexure, stress, and twist. We assign support forces, S<sub>1</sub> and S<sub>2</sub>, on the right rigid frame, and similarly, S<sub>3</sub> and S<sub>4</sub> on the left frame as torque components. Fig. 7 shows the conditions after assigning the values required to start the calculation.

All the support forces are assigned as torques operating on rigid frames in our model. In addition, the pivot joints allow free axial slide and rotation without changing their positions. Once the FEM program starts, we can obtain the scalar quantities of flexure and stress (von Mises force). The data are concerned with the landing section normally, but are not limited to any chassis positions where we designate. As a result, we have the final displays of stress and flexure, shown in Fig. 8. Suppose that the i-th landing section, and force in mm and kilogram dimensions are P<sub>i</sub>(x, y, z) and S<sub>i</sub>(f), respectively. Then, the values in the figure are such that: P<sub>1</sub>(–225,320,0), P<sub>2</sub>(225,–240,0), P<sub>3</sub>(–225,320,0), P<sub>4</sub>(–225,–160,0) and S<sub>1</sub>(5.10), S<sub>2</sub>(0.51), S<sub>3</sub>(0.10), S<sub>4</sub>(13.27). The material is aluminum and its physical parameters are thickness, 3 mm(=t), Poisson's ratio, –0.33(=ν), strength of extension and compression, 250 MPa. In addition, the

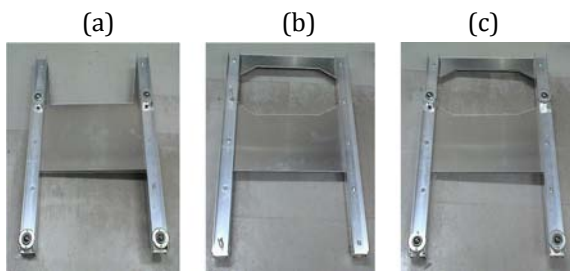


**Fig. 9. Assembled chassis with rigid edges: (a) is BR-type; (b) and (c) are SL-type; (b) is a top view and the others are bottom views, i.e., upside-down**

segmentation size is 2.5 mm, and the number of knots and elements are 204643 and 107145, respectively. In the calculation, von Mises force ( $\sigma$ ) and flexure ( $E$ ) are utilized [5, 11]. The maximum value of flexure must be less than the breaking point of stress. Hence, the application is not practical when actual stress reaches the breaking point.

We used a PC (Sony Vaio VGN-Z 2.8 GHz; Vista RAM 4 GB) for the calculation of the analysis using the model. It took approximately 17 minutes to calculate the results, and showed bends and twists according to the chassis types with quantitative amounts. The transient flexures and stresses continuing to their final states shown in Fig. 8 are observed as an animation.

## 5. Verification of Static Flexure Analysis

### 5.1. Fabricated Chassis and Experimental Set

Some of the fabricated chassis are illustrated in Fig. 9. The landing sections of the chassis have spherical casters so that it can move as if in a practical environment. In all chassis types, the front and rear casters are located at a distance of 30 and 190 mm, from the front and rear frame edges, respectively.

We obtained the data for flexure at the right front section of the chassis using the BR-type. Fig. 10 shows an experimental setup that can steadily lift a certain section to measure its height with an electric scale on the experimental board. The right part is the front of the chassis.

We set conditions such that two pairs of two rods connect the left and right rigid chassis frames. Each pair of rods is guided into spherical joints to make the chassis free from bending, stretching, and twisting. A load of cargo, like seating boards, is intended to be put on these rods (see Fig. 4). The dummy weights on the front and rear pairs of the rods are 15.00 kg and 19.82 kg, respectively. Each pair of rods and spherical joints weigh 0.75 kg and 0.98 kg on one side. Since the chassis has a symmetrical form in both sides and each pairs of rods are displaced from the chassis center with the distance 116 mm and  $-160$  mm along the Y-axis, the total load operating on the rigid frame is calculated at a backward position from the chassis center with the distance 41.10 mm. The load  $S$  assigned in Fig. 6 has the value of 19.14 kg ( $= (15.00 + 19.82) / 2 + 0.75 + 0.98$ ).

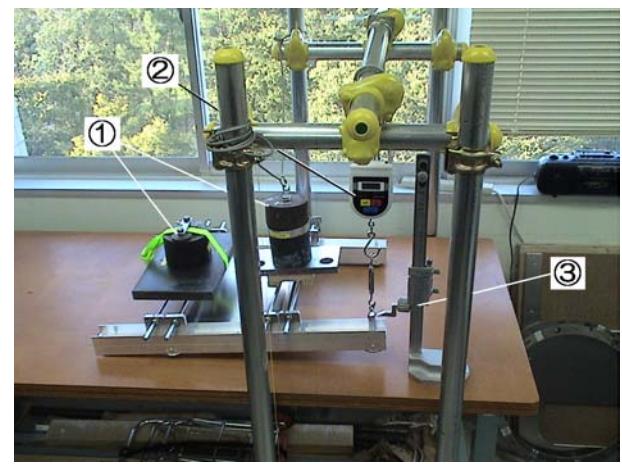


**Fig. 10. Overview of the experimental setup that measures flexure while changing the lift force at the right rear of the chassis. Circled numbers from 1 to 6 refer to dummy weight, electric spring gauge, height gauge, turnbuckle, spherical joint, and spherical caster, respectively**

We apply a lift force to the right front or right rear sections of spherical casters that can move freely on the experimental board; that is, the framework hooks an electric spring gauge, turnbuckle, and the section of the chassis being measured in series. Then, the lift force displayed on the gauge is changed arbitrarily by altering the length of the turnbuckle. Simultaneously, the vertical displacement of the section is manually measured from the plane on which the other landing sections exist (i.e., the surface of the experimental board) using a height gauge with an accuracy of 0.1 mm.

Figs. 11(a)–(c) show the results using the simple chassis forms of thickness, 2 mm. Clearly, flexure of the front and rear sections are located at the left and right areas due to the amount of lift force. Each figure also shows the analytical results. Actually, in the rear section lift, the model shown in Fig. 6 is utilized. Fig. 12 shows the 3D chassis deformed under the lift force of  $S = 7$  kg which is dealt with in Fig. 11. Clearly, analytical and experimental results are very close in Fig. 11. These results validate that the proposed models are reasonable.

In the verification of the model in Section 4.3, the lift force might be assigned, similarly to the measurement manner in Section 4.2. However, we place short platform scales, that is, bathroom scales, under the spherical casters and adjust the height by placing the platform scales on height adjusting stands so that the scale indicates the assigned value. Then we verified

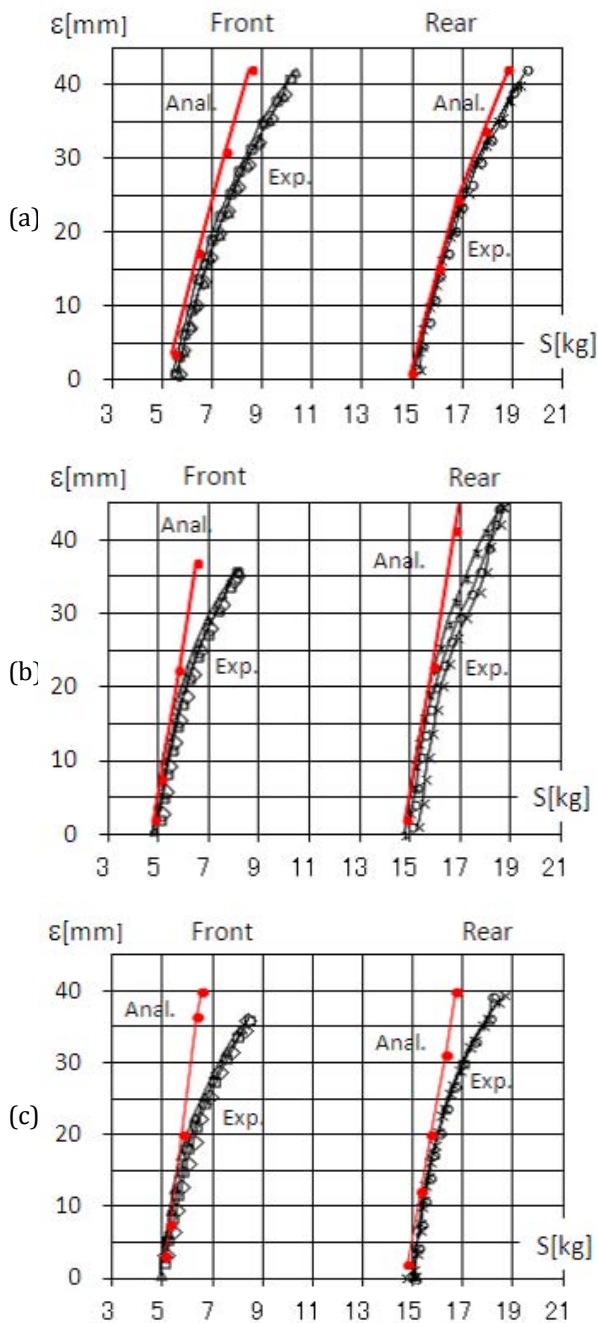


**Fig. 11. Comparison of the experimental and analytical characteristics of flexure versus lift force. (a), (b), and (c) are concerned with types of BR, LL, and SL, respectively. Material of (a) is stainless, and those of (b) and (c) are aluminum. All materials are 2 mm in thickness**

that the chassis deformed similarly to the form obtained by the FEM. In addition, we confirmed that the chassis twisted according to the results of the calculation depending on the amount force of assigned. These results are not shown due to complexity.

**5.2. Comparison of Flexures Depending on the Chassis Thickness**

The amount of flexure depending on the thickness of a chassis made of aluminum is compared in Fig. 13. The symbolic notation, t2, t3, and t4 represent the di-

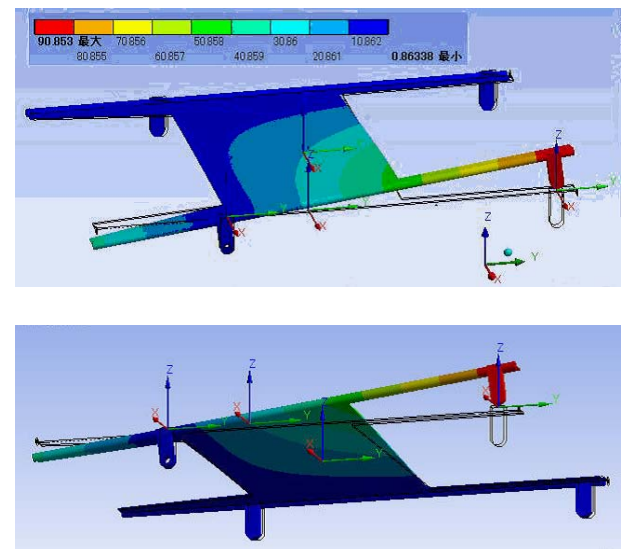


**Fig. 12. Analytical results of flexure for the case shown in Fig. 10 while lifting the right front side with  $S = 7$  kg. The upper side and lower side are the views from the top and bottom, respectively. The lower side corresponds to the bottom photo in Fig. 10**

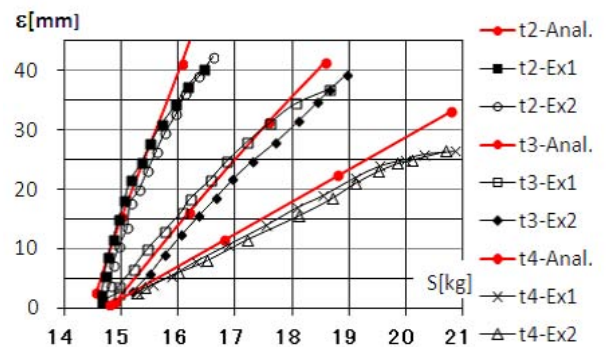


**Fig. 13. Comparison of the experimental and analytical characteristics of the BR-type chassis flexure depending on the thickness of the aluminum**

mensions of 2 mm, 3 mm, and 4 mm, respectively. Clearly, flexure decreases as the thickness increases. In addition, analytical and experimental results are close.

**5.3. Comparison of Flexure Depending on the Chassis Material**

We applied the FEM to calculate flexure of chassis that all have the same BR-type, and  $t=3$  mm,  $e=3$  mm. Seven materials are considered: magnesium alloy, aluminum alloy, titanium alloy, copper alloy, gray cast iron, stainless steel and alloy steel. The data in Fig. 14 show the results for these materials in the given order from top to bottom. From the verification of likeness between experimental and analytical data shown in Fig. 12, we can guess that the flexure of other materials might be close to the analytical data without

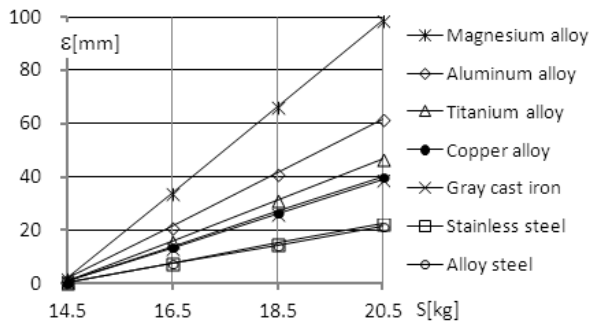


**Fig. 14. Analytical characteristics of the BR-type chassis flexure depending on materials of thickness, 3 mm. For visibility, experimental data are not shown**

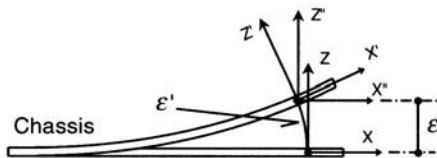


**Fig. 15. Difference of the flexure in analytical and experimental results. Clearly,  $E$  becomes less than  $E'$  according to the increase of  $S$**

collecting practical flexures. The above-mentioned results, including the physical parameters, are summarized in Table 1. One can find that the materials are aligned in ascending order of virtual spring constant of the chassis.

**5.4. Discussion on the Error of Flexure in Analytical and Experimental Results**

In the experiment, the chassis flexure is read as the height of the measurement section from the experimental board in the coordinate system (X, Y, Z) which is common on the board. However, chassis plane inclines according as the lifting force at the section increases and the positive direction of Z-axis changes to yield that small displacements are accumulated for making a curved flexure. This is based on the fact that the Z-axis is always normal to the chassis in the analysis. Suppose the measurement in X-Z plane, then the curved flexure  $E'$  meaning the analytical flexure is shown in Fig. 15. This is the reason why the analytical data are linear to the lifting force. Small errors appearing according to the increase of  $S$  in Figs. 11 and 13 are now understandable.

**6. Analysis of the Chassis Dynamics**

Static analysis of the chassis has been described so far. This section pursues the dynamics of the chassis since its behavior is important to restrict vibration when the robot starts, stops or moves with an influence of external disturbances.

**6.1. Preparation of the Modal Analysis**

Basically, the structural model of the chassis is similar to those shown in Section 4. However, typical char-

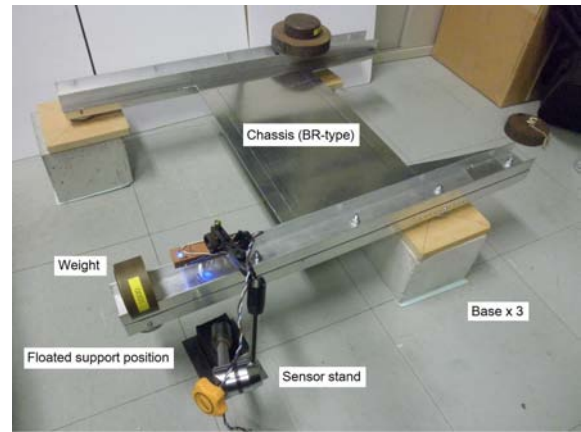


**Fig. 16. Experimental setup for measuring the natural frequency of the BR-type chassis**

acters of the dynamics exist in such patterns of time-dependent deformation and natural frequency of the chassis vibration. These are expressions of an intrinsic physical phenomenon. Therefore, the torque-force operation in the static analysis is reviewed as a torque-displacement operation. In such the case when some weight operates on a certain section of the chassis, the weight might be embedded into the chassis by supposing that the volume of the weight is negligible small. Otherwise, the weight needs to be processed as a structural component of the chassis. In order to simplify the calculation, we consider that the weight is a point-like mass with high density fixed on the rigid frame.

**6.2. Experimental Setup and Experiments for Clarifying Modal Characteristics**

Suppose that the experiment is dealt with the BR-type chassis. Then the experimental setup including optical devices for measuring the natural vibration is overviewed in Fig. 16. The sensor stand hooks an optical pair of emitting and receiving over the vibrating target. The role of the pair is to count the chassis vibration, no matter how the vibration mode is complex. We built the optical sensor by assembling such devices of the LED, E1L33-3B ( $\lambda=450\text{nm}$  Toyoda Gosei Co.Ltd.), and the photo transistor, TPS603 (Toshiba Corp.). Optical axes cross at  $90^\circ$  so that an optical target is sensed in the vicinity of the distance, 5cm. Other instruments that are not shown in the figure are ready for the measurement. They are digital storagescope, DS-8710 100MHz (IWATSU Electric Co. Ltd.) and thermal printer, DPU-411 (Seiko Instruments Inc.) communicating via serial ports.

In Fig. 16, one support section of the chassis is free, because the chassis stands on only three bases. When we pat the free rigid frame, the chassis begins to vibrate. Actually, such vibration signals shown in Fig. 17 are monitored. In an analytical points of view, three flexures shown in Fig. 18 are calculated under the modes of 1, 2 and 3 that are related to bending, twisting and complex bending patterns, respectively. Also, calculated results of natural vibrations in modes

**Tab. 1. Physical parameters and evaluated elasticity of seven materials intended for 3 mm-thick chassis**

Material	Density [g/cm <sup>3</sup> ]	Young's Modulus [Pa]	Poisson's Ratio	Yieldforce Ten./Com. [MPa]	VonMises Stress Max.[MPa]	Maximum Flexure [mm](= Z)	Suspension Springconst. [g/mm]
1)Magnesium	1.80	4.50E + 10	0.35	193/193	100.51	98.709	61.828
2)Aluminum	2.77	7.10E + 10	0.33	280/280	101.31	61.847	98.679
3)Titanium	4.62	9.60E + 10	0.36	930/930	100.10	46.533	131.154
4)Copper	8.30	1.10E + 11	0.34	280/280	100.92	40.150	152.005
5)Gray cast	7.20	1.10E + 11	0.28	240/820	103.25	38.750	157.497
6)Stainless	7.75	1.93E + 11	0.31	207/207	102.11	22.487	271.401
7)Alloy steel	7.85	2.00E + 05	0.30	250/250	102.50	21.571	282.926

Lift force is 6.1[kg] at the right rear of the chassis

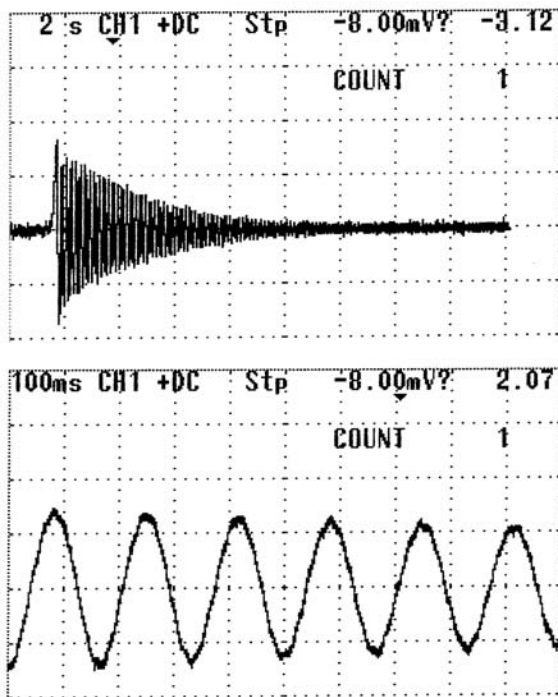


**Fig. 17. The setup in Fig. 15 produced the form of a chassis vibration. In the top, an impulsive distortion is given to a rigid frame of the chassis. The sweep range 2 s/div in the top are changed to 100 ms/div to have the vibration form in the bottom. The chassis is made by aluminum of thickness, 3 mm. Clearly, the frequency, 6 [Hz] is measured**

of 1 and 2 among seven materials shown in Table 1 are compared. However, the vibrations in Fig. 17 reveals that the flexures in the modes of 2 and 3 are negligible. Therefore, we calculated the natural frequency only in the mode 1. And we collected not only the natural frequency of the chassis itself but also the chassis when some amount of weight operates on the floated section.

Finally, calculated and experimental results of the vibration frequency are shown in Fig. 19. From the figure, it is confirmed that the form of the vibration is almost assumed as that in the mode 1. In the experiment, we could confirm that the frequency of

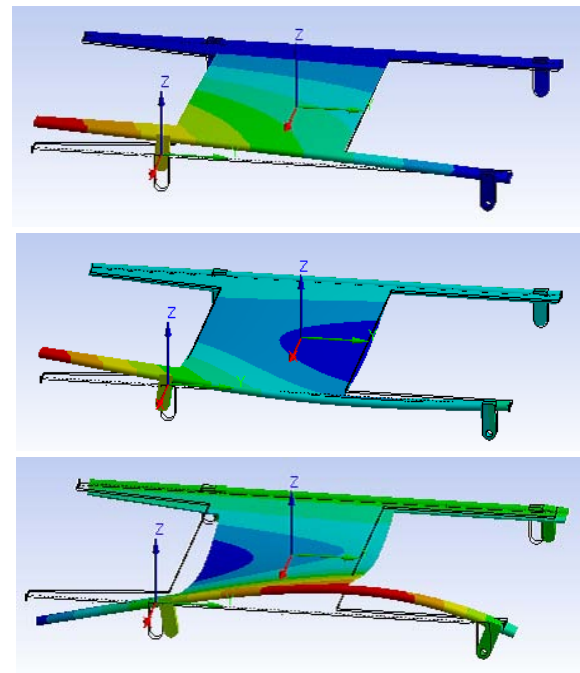


**Fig. 18. Three flexure patterns considered in the modal analysis. Vibration modes from the top to the bottom are 1, 2 and 3**

the vibration increases and the vibration amplitude decreases faster according as the material becomes thicker. These results verify that the modal analysis using the FEM is quite good to explain the actual vibration.

## 7. Influence of Long Air Space Patterns

The calculation program using the chassis model makes it possible to determine the mechanical characteristics of chassis stress and flexure. Of course, it is possible to understand the influences arising from differences in the amount, direction, and breadth of long air space, in addition to the difference in Young's constant, and Poisson's ratio. The maximum values of  $\sigma$  and  $E$  are calculated on different types of chassis shown in Figs. 2(d)–(f) and Figs. 20(a)–(f) under the same conditions; that is, the material is alu-

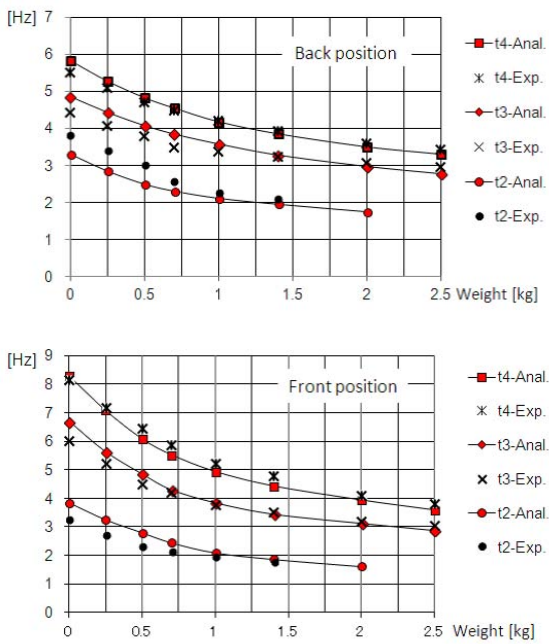


**Fig. 19. Analytical and experimental results of the natural frequency of the BR-type chassis under the uniformness of the material; steel alloy. The data in the top and bottom are concerned with the rear and front support sections of the chassis, respectively**

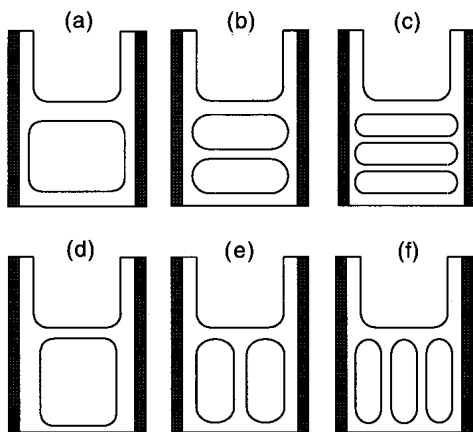


**Fig. 20. Different chassis with long air holes that are distinguished by the types H1, H2, H3, V1, V2, and V3**

minum of 3 mm, space exclusion of 21.4% (49.8% when including the seating area), circular radius of 25 mm, and segmentation size of 3 mm. The results are shown in Fig. 21, where we label the chassis types in Figs. 20(a)–(f) H1, H2, H3, V1, V2, and V3 after the attribute of horizontal or vertical directions and the amount of long air space. All data are collected by lifting the right rear section (see Fig. 6). In Fig. 21, the V3-type is excluded because the maximum of  $\sigma$  became bigger than the breaking point of aluminum.

Due to no common rules about the position of long air space, a comparison of the results mentioned previously is difficult in general. However, it is clear that the number of long air spaces influences the V-type

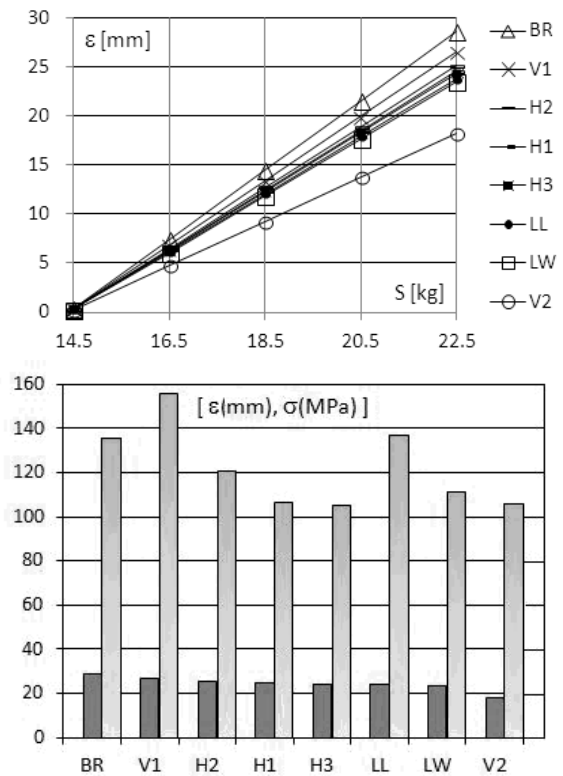


**Fig. 21. Top: Analytical results of flexure versus chassis forms when the eight long air space patterns are considered under the conditions such that the front section of the chassis is lifted. Bottom: Analytical results of both flexure (left bar) and stress (right bar)**

rather than the H-type, on the whole. In addition, the V-type is more suitable for making a flexible chassis compared to the H-type, but the type has a tendency to increase stress for a chassis.

Fig. 20 has no chassis type that arranges long air spaces parallel to a shift of half its length toward the vertical or horizontal directions. In addition, it excludes the case where the chassis has many circular holes. These are based on our considerations that the totally removed area is not enough to make the chassis light, while keeping  $\sigma_{max}$  smaller than the yield point of the chassis material.

### 8. Conclusion

This paper proposed a chassis design concept of a mobile robot. The idea is to change the chassis from a rigid plate to an elastic plate and to remove some area. The trimmed-down chassis makes the robot slim, lightweight, maintenance-free, and efficient in saving power. For analyzing the behavior of a chassis section, we pursued mechanical chassis models that are directly introduced to the calculation of the FEM. These models are applicable to estimate stress and flexure for a variety of chassis types. Also, the dynamic chassis behaviors are analyzed using the FEM. Results of the analysis became similar to those of the experiments. Therefore, the proposed structural models are beneficial to evaluate various chassis in size and thickness for optimization before practical robot designing.

At the beginning of this study, angular and circular air spaces were considered for cutting. However, these profiles made it difficult to remove a wide area in total without weakening the strength of the chassis. The allocation of long air spaces is roughly assigned without considering their precise positions. Therefore, our next subject is to study the geometry of long air spaces. In practical designs, many factors such as material cost, manufacturing cost, total load, total weight, and corrosion resistance might be influential to design thick chassis with large air space or thin chassis with small air space.

## ACKNOWLEDGEMENTS

This study was partially supported by a grant from KAKENHI (C24560287).

## AUTHORS

**Tokuji Okada\*** – Niigata University, 2-8050 Ikarashi, Niigata-shi, Niigata, Japan 950-2181, e-mail: okada@eng.niigata-u.ac.jp, www: http://okada@eng.niigata-u.ac.jp.

**Nobuharu Mimura** – Niigata University, 2-8050 Ikarashi, Niigata-shi, Niigata, Japan 950-2181, e-mail: mimura@eng.niigata-u.ac.jp, www: http://mimura@eng.niigata-u.ac.jp.

**Toshimi Shimizu** – Ibaraki University, 4-12-1 Nakanarusawa, Hitachi-shi, Ibaraki, Japan 316-8511, e-mail: toshimi@mx.ibaraki.ac.jp, www: www.mech.ibaraki.ac.jp/en.

\*Corresponding author

## REFERENCES

- [1] *Handbook on Car Engineering*, vol.II Chap.5 "Suspension" (pp. 1–15), "Leveling" (pp. 30–33), Rikogaku Inc., May, 2005, . (in Japanese).
- [2] M. Fujiwara, W. Mizunuma, A. Shinozaki, "Automatic Guided Vehicle for Outdoor Use", *J. Robotics Society*, vol.18, no.7, October 2000, 955–960,(in Japanese).
- [3] T. Okada, A. Mahmoud, W. Botelho, T. Shimizu, "Trajectory estimation of a skid-steering mobile robot propelled by independently driven wheels", *J. ROBOTICA*, vol.30, no.1, 2012, 123–132.
- [4] T. Okada, W. T. Botelho, T. Shimizu, "Motion analysis with experimental verification of the hybrid robot PEOPLER-II for versatile switch between walk and roll on demand", *Int. J. Robotics Research*, vol. 29, no. 9, August 2010, 1199–1221.
- [5] "ANSYS Workbench Mechanical Introductory Seminar", Edited by Cybernet Co. Ltd, April, 2012 (in Japanese).
- [6] R. Sancibrian, P. Garcia, F. Viadero, A. Fernandez, A. DeJuan, "Kinematic design of double-wishbone suspension systems using a multiobjective optimisation approach", *Vehicle System Dynamics: Int. J. of Vehicle Mechanics and Mobility*, vol.48, no.7, July 2010, 793–813.
- [7] J-S. Zhao, L. Li, L. Chen, and Y. Zhang, "The concept design and dynamics analysis of a novel vehicle suspension mechanism with invariable orientation parameters", *Vehicle System Dynamics: Int. J. of Vehicle Mechanics and Mobility*, vol.48, no.12, Dec., 2010, 1495–1510.
- [8] X. Shen, F. Yu, "Investigation on integrated vehicle chassis control based on vertical and lateral tyre behavior correlativity", *Vehicle System Dynamics: Int. J. of Vehicle Mechanics and Mobility*, vol.44, Supplement, 2006, 506-519.
- [9] E. H. Mansfield, *The Bending and Stretching of Plates*, Cambridge University Press, 2010.
- [10] K. Yoneda, T. Kuga, "Quadruped robot with reduced number of actuators", *J. of RSJ*, vol. 22, no. 7, Oct. 2004, 946-952. (in Japanese).
- [11] "ANSYS Analyzing soft using FEM", Edited by CAD/CAM Kenkyukai, Rikogaku Inc., May, 2005 (in Japanese).